Flow patterns in carotid webs: a patient-based computational fluid dynamics study

Kars C.J. Compagne, Kristina Dilba, Erik Jan Postema, Adriaan C.G.M. van Es, Bart J. Emmer, Charles B.L.M. Majoie, Wim H. van Zwam, Diederik W.J. Dippel, Jolanda J. Wentzel, Aad van der Lugt and Frank J.H. Gijsen, for the MR CLEAN investigators.

AJNR Am J Neuroradiol. 2019 Apr;40(4):703-708.

ABSTRACT

Background and purpose Carotid webs are increasingly recognized as an important cause of (recurrent) ischemic stroke in patients without other cardiovascular risk factors. Hemodynamic flow patterns induced by these lesions might be associated with thrombus formation. The aim of our study was to evaluate flow patterns of carotid webs with the use of computational fluid dynamics (CFD).

Material and methods Patients with a carotid web in the MR CLEAN-trial were selected for hemodynamic evaluation with CFD models based on lumen segmentations obtained from CT-angiography scans. Hemodynamic parameters including area of recirculation zone, time-averaged wall shear stress (TAWSS), transverse WSS (transWSS) and oscillatory shear index (OSI) were assessed and compared to the contralateral carotid bifurcation.

Results In our study, 9 patients were evaluated. Distal from the carotid webs, recirculation zones were significantly larger compared to the contralateral bifurcation (63 versus 43 mm^2; p 0.02). In the recirculation zones of the carotid webs and the contralateral carotid bifurcation TAWSS values were comparable (both median 0.27 Pa; p 0.30) while transWSS and OSI values were significantly higher in the recirculation zone of carotid webs (median 0.25 Pa versus 0.21 Pa; p 0.02 and 0.39 versus 0.30 Pa; p 0.04]). At the minimal lumen area, simulations showed a significantly higher TAWSS in the web compared to the contralateral bifurcation (median 0.58 versus 0.45 Pa; p 0.01).

Conclusions Carotid webs are associated with increased recirculation zones and regional increased WSS metrics that are associated with disturbed flow. These findings suggest that a carotid web might stimulate thrombus formation which increases the risk of acute ischemic stroke.

INTRODUCTION

Carotids webs are fibrous shelf-like lesions causing narrowing in the proximal internal carotid bulb. Although these lesions are rare, carotid webs are an important cause of (recurrent) ischemic stroke in patients without cardiovascular risk factors [1, 2]. Previous studies reported that carotid webs are more frequently observed in younger females, and are associated with a high risk of recurrent ischemic stroke [1, 3]. The underlying mechanism for the association between carotid webs and stroke is unknown, but it was speculated that the impact of the web morphology on flow patterns might lead to thrombus formation [1], nonetheless this has never been studied.

Hemodynamic flow patterns have been extensively studied in atherosclerotic carotid artery by computational fluid dynamics (CFD) [4-7]. This computer-based technique simulates fluid flow patterns based on the Navier-Stokes equations. Using image-based geometry of vessels, boundary conditions and fluid properties, it is possible to simulate hemodynamic patterns. For example, areas of recirculation of blood flow can be investigated and quantified. These recirculation zones are observed in healthy carotid bifurcations, but increase in size distal from a stenosis [8-13]. In addition, frictional force induced by the blood flow (i.e. wall shear stress (WSS)) can be investigated by CFD models. WSS affects many pathophysiological processes related to atherosclerosis and is associated with ischemic stroke [4, 14]. Several WSS derived parameters may be of interest in patients with webs. Time-averaged WSS (TAWSS) describes the wall shear stress magnitude over a cardiac cycle. Lower TAWSS values might stimulate atherosclerosis while high values can cause endothelial trauma [4]. Evaluating transverse WSS (transWSS) gives the opportunity to quantify multidirectional flows [15]. TransWSS is the average of all WSS components perpendicular to the mean flow direction, consequently taking multi-directionality into account. This recently defined metric corresponds with the location of atherosclerotic lesions [16].Finally, oscillatory shear index (OSI) can be assessed to characterize temporal variability of WSS during a cardiac cycle [17]. Larger changes in the direction of WSS during a cardiac cycle results in a higher OSI and is associated with atherogenesis [18].

Both carotid webs and atherosclerotic stenosis are narrowing the lumen at the level of the carotid bifurcation. However, the hemodynamic profile may not be comparable due to differences in 3D morphology. In general, at the proximal part of both lesions the lumen becomes gradually smaller. However, the lumen distal from the carotid webs differs from an atherosclerotic stenosis due to the shelf-like fibrous lesion, which may greatly influence the distal flow patterns. Gaining insight into the flow patterns of carotid webs might improve the understanding of the risk of (recurrent) ischemic stroke in patients with carotid webs.

In this study, we evaluated simulated flow patterns of carotid webs in patients with acute ischemic stroke with the use of patient-based CFD and compared these to the flow patterns in the contralateral carotid bifurcation.

MATERIAL AND METHODS

Patients and imaging data

Patients were selected from the Multicenter Randomized Clinical trial of Endovascular treatment of Acute Ischemic stroke in the Netherlands (MR CLEAN trial) [19]. Briefly, patients were included in the MR CLEAN trial (n=500) if a proximal intracranial arterial occlusion was radiographically confirmed, and had a minimum score of 2 on the National Institutes of Health Stroke Scale (NIHSS) at baseline. The study protocol was approved by a central medical ethics committee and the research board of each participating center. Written informed consent before randomization was provided by all patients or their legal representatives.

Patients with a carotid web (n=9) had a CTA scan with a slice increment of 0.5 mm and an average in-plane resolution of 0.46×0.46 mm^2. Stenosis measurements on CTA were semi-automatically performed by a cross-sectional area measurement at the level of the narrowest lumen divided by the disease-free area distal from the lesion.

Segmentation and meshing

Semi-automated segmentations of both carotid arteries using a region growing algorithm was performed with open source DICOM viewer Horos (version 2.0.1) [20]. Due to different rates of contrast load in each CTA scan, the threshold intensity value was chosen for each patient based on best representation of morphology by one observer (KC). Vascular side branches and remaining calcifications were removed from the 3D volume rendered lumen. The final segmentation included common carotid artery, external carotid artery and internal carotid artery. Flow extensions were added with a length of three diameters at the inlet and both outlets. Volumetric meshes of tetrahedral elements and prism layers were generated using ANSYS ICEM CFD software 17.1. Number of elements ranged between 2.45×10^6 and 7.80×10^6 with a minimal and maximal element size of 0.05 mm and 0.15 mm, respectively.

Computational fluid dynamics and analysis

A plug-like inflow profile was chosen. The average inlet velocity was calculated as a function of the diameter to obtain a wall shear stress of 1.2 Pa at the inlet flow extension [21]. Due to absence of patients specific boundary conditions and since no significant stenosis (<50%) was present the, outflow-ratios for internal and common carotid artery

(resp. ICA and CCA), and external (ECA) and CCA were assumed to be respectively 0.65 and 0.35 [22]. Blood was modelled as an incompressible fluid with a density of 1.06 g/cm3, and the Carreau model was applied to account for the non-Newtonian shear thinning behavior [23]. Time-dependent simulations were performed, using a generic flow wave form shapes as proposed by Lee et al [24]. Two cardiac cycles were included, with a time step of 0.01 seconds. Since the first cycle potentially contains numerical artefacts, only the results of the second cycle were used for the analyses.

From the time-dependent simulations, various hemodynamic parameters were extracted: TAWSS, transWSS and OSI. 2D TAWSS maps were created and used to determine the region of reversed flow (recirculation zone). Subsequently, the total surface area (mm^2) and length (mm) of the recirculation zone was computed [25]. Furthermore, TAWSS was assessed at the minimal lumen area of the carotid web or stenosis and in the recirculation zone. TransWSS and OSI were both assessed in the recirculation zone (Suppl. Figure 1). TransWSS was introduced by Peiffer et al as follows [15]:

$$transWSS = \frac{1}{T}\int_0^T \left| \vec{\tau}_\omega \left(\vec{n} \frac{\int_0^T \vec{\tau}_\omega dt}{\left| \int_0^T \vec{\tau}_\omega dt \right|} \right) \right| dt$$

$\vec{n}$ represent the normal to the arterial surface.

For illustration purposes, streamlines were created based on the time-average velocity field. All CFD simulations were performed within ANSYS Fluent 17.1, using standard numerical techniques.

Statistical analysis

Descriptive statistics of the characteristics of flow patterns were presented as median and interquartile ranges (IQR) due to a non-normal distribution. Hemodynamic parameters of flow patterns in carotid bifurcations with a web were compared to the contralateral carotid bifurcation (control group) within patients and evaluated with a paired Wilcoxon signed-rank test. Degree of stenosis was correlated with the length of the recirculation zone using a Spearman rank correlation test. Statistical analyses were performed using R Studio (version 3.4.2) and packages haven, Hmisc, foreign, ggpaired and ggpubr.

RESULTS

Included patients were mostly female (n=8 (91%)) with a median age of 59 years [IQR 45-70]. All patients had a carotid web in the symptomatic carotid bifurcation of acute ischemic stroke, except for one patient where the carotid web was located in the asymptomatic carotid bifurcation. One patient had a history of atrial fibrillation (Table 1).

Table 1. Baseline characteristics of included patients

Case	Gender, age	Carotid web in symptomatic bifurcation	Location intracranial occlusion	Previous stroke	Smoking	Diabetes mellitus	Atrial fibrillation	Myocardial infarction
1	F, 45	Yes	M1 right	Yes	No	No	No	No
2	M, 77	Yes	M1 right	No	No	No	Yes	No
3	F, 67	Yes	M1 right	No	No	No	No	No
4	F, 44	Yes	ICA-T right	No	No	No	No	No
5	F, 66	Yes	M2 right	No	No	No	No	No
6	F, 45	Yes	ICA-T right	No	No	No	No	No
7	F, 59	Yes	M1 right	No	No	No	No	No
8	F, 46	Yes	M1 right	No	No	No	No	No
9	F, 73	No	M1 left	No	No	No	No	No

ICA-T, ICA terminus.

A representative case of a carotid artery web is shown in Figure 1. The streamlines show that in the region distal from the carotid web a large recirculation zone is observed. Furthermore, at the minimal lumen area at the location of the web, a high TAWSS is observed.

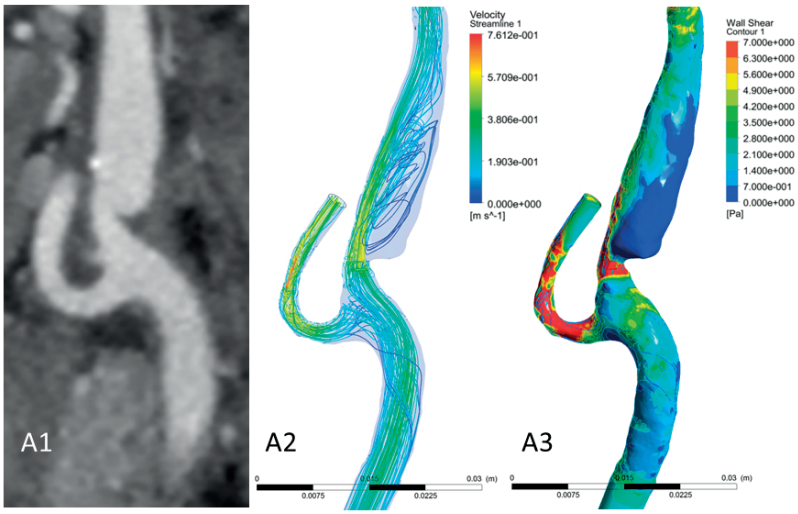

Figure 1. A case with a carotid web in the ipsilateral carotid bifurcation of an ischemic stroke patient. Images of CTA (**A1**) and CFD simulations (**A2**, streamlines; **A3**, wall shear stress (WSS)). Focused on the region distal from the carotid web, a large recirculation zone is observed with low time-averaged WSS (TAWSS) values. At the minimal lumen area at the location of the web, a high TAWSS is observed. Streamlines were based on time-averages velocity field.

Results of the CFD simulation of the carotid bifurcations are summarized in Table 2 (Suppl. Figure 2). Severity of stenosis caused by the web varied from 13 to 70%. At the contralateral carotid bifurcation, stenoses were observed in 3 patients (range 14-56%). In both carotid arteries with webs as well as in the contralateral carotid arteries, recirculation zones were observed. However, total surface and length of recirculation zone were significantly larger in carotid bifurcation with a web compared to the contralateral carotid bifurcation (mean within-patient difference 38 mm^2 and 6 mm, respectively) (Table 2 & Figure 2, panel A). This difference was present in all patients except in the patient who had a web in the asymptomatic carotid bifurcation (Suppl. Table 1). TAWSS in the recirculation zones of carotid bifurcations with webs and in the contralateral carotid bifurcation did not significantly differ. Maximum transWSS values were significantly higher in the recirculation zones distal from the carotid web (mean within-patient difference 0.09 Pa; 87%) (Figure 2, panel B). Likewise, OSI values were significantly higher in the recirculation zones in the carotid bifurcation with webs (mean within-patient difference 0.12; 55%) (Figure 2, panel C). At the minimal lumen area at the

location of the carotid web, simulations showed a significantly higher maximum TAWSS compared to the contralateral bifurcation (mean within-patient difference 0.20 Pa; 44%) (Figure 2, panel D).

Table 2. Results of hemodynamic parameters between carotid web and contralateral carotid bifurcation.

	Carotid web	Contralateral carotid bifurcation	P-value
Recirculation zone			
Area (mm^2)–median [IQR]	63.61 [50.60-99.38]	43.0 [36.46-50.34]	0.02
Length (mm)–median [IQR]	6.90 [5.60-8.60]	1.80 [1.40-2.10]	0.01
Mean TAWSS (Pa)–median [IQR]	0.27 [0.23-0.34]	0.27 [0.22-0.28]	0.30
Maximum transWSS (Pa)–median [IQR]	0.25 [0.20-0.31]	0.21 [0.10-0.23]	0.02
Maximum OSI –median [IQR]	0.39 [0.36-0.43]	0.30 [0.19-0.33]	0.04
At level of minimum lumen area			
Maximum TAWSS (Pa)–median [IQR]	0.58 [0.51-0.61]	0.45 [0.34-0.47]	0.01

P values were obtained from a paired Wilcoxon signed-rank test. TAWSS, time-averaged wall shear stress; transWSS, transverse wall shear stress; OSI, oscillatory shear index.

In the carotid bifurcations with a web, no correlation between degree of stenosis and surface or length of the recirculation zone was observed (ρ=0.23; p 0.55 and ρ=0.27; p 0.49, respectively).

DISCUSSION

This study provided insight into the flow patterns associated with carotid webs in the carotid bifurcation. We observed that carotid webs show increased recirculation zones with corresponding higher OSI and transWSS values compared to the contralateral carotid bifurcation in patients with acute ischemic stroke. Furthermore, at the minimal lumen area higher maximum TAWSS values were observed in the carotid bifurcation with a web.

Recirculation of blood is associated with an increase in platelet deposition and aggregation, which could lead to thrombogenesis over time [26]. All patients in our study had a larger total surface of recirculation in the bifurcation with a carotid web compared to the contralateral side, except in one patient who had a web in the asymptomatic carotid bifurcation. In our study, we did not find a significant association between length or total surface of recirculation zone and degree of stenosis caused by a carotid web. It is well possible that the degree of stenosis does not reflect the complex geometry distal from the stenosis, which is the main driver of the hemodynamic patterns.

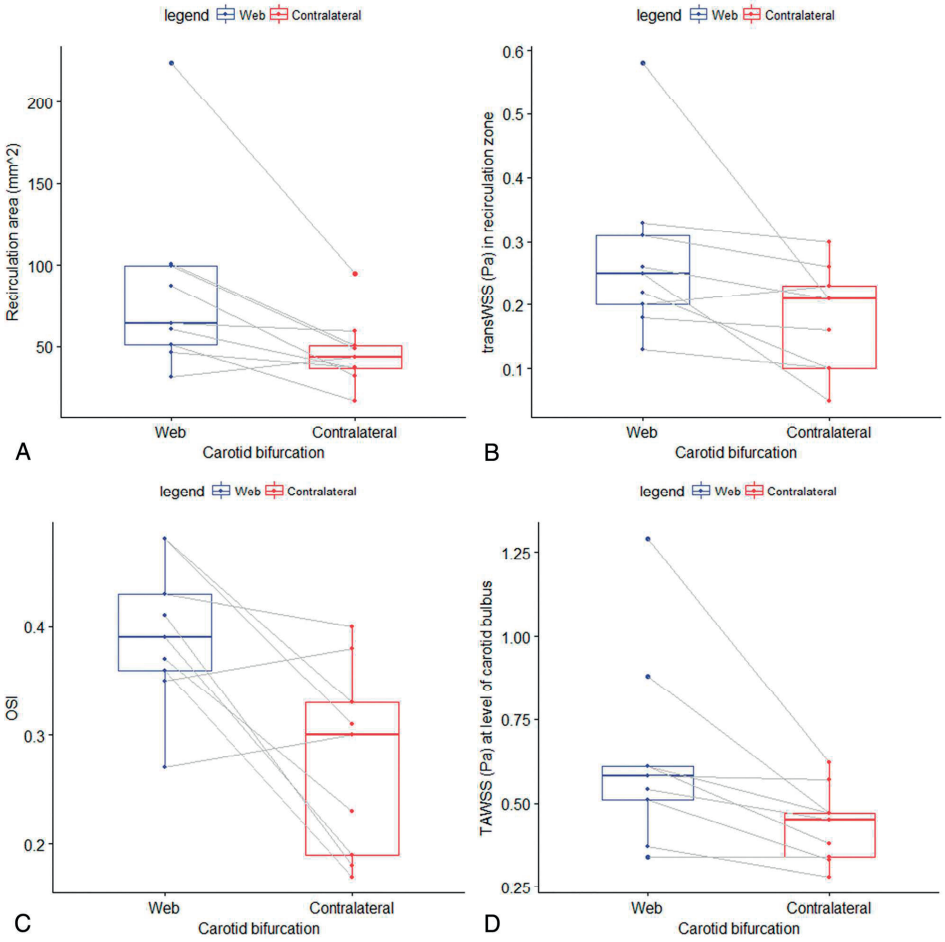

Figure 2. Boxplots showing the distribution of total surface of recirculation zone, transWSS, OSI and TAWSS for the carotid bifurcation with a web and contralateral bifurcation. P values were obtained from a paired Wilcoxon signed-rank test. **Panel A:** Distribution of total surface of recirculation area which was statistically significant (p 0.02) larger in carotid bifurcations with a web compared to the contralateral carotid bifurcation (control group) within patients. **Panel B:** Distribution of transverse wall shear stress (transWSS) in the recirculation zone which was statistically significant (p 0.02) larger in carotid bifurcations with a web compared to the contralateral carotid bifurcation (control group) within patients. **Panel C:** Distribution of maximum Oscillatory Shear Index (OSI) in the recirculation zone which was statistically significant (p 0.04) larger in carotid bifurcations with a web compared to the contralateral carotid bifurcation (control group) within patients. **Panel D:** Distribution of maximum time-averaged wall shear stress (TAWSS) (Pa) at the level of the carotid bulbus which was statistically significant (p 0.01) larger in carotid bifurcations with a web compared to the contralateral carotid bifurcation (control group) within patients.

We observed a high maximum TAWSS at the site of minimal lumen area caused by the carotid web. This finding has also been observed proximal to the minimal lumen area in patients with a stenosed artery due to atherosclerosis [4, 21, 27]. In perspective, healthy persons have an averaged WSS in carotid arteries of approximately 1.2 Pa [21]. However, in recirculation zones, low WSS is characteristically common[28]. Vascular walls exposed to low WSS are prone to atherosclerosis and platelet aggregation, while high WSS induces platelet activation [4, 29]. Despite similar TAWSS values in the recirculation zones of carotid bifurcations with webs and their contralateral carotid bifurcations, higher transWSS and OSI values in carotid bifurcations with a carotid web were observed. These observations represents a multidirectional disturbed blood flow, which might be prone to vascular wall dysfunction [30]. Along with the fact that larger recirculation zones promote platelet aggregation to the endothelium, shear-induced activated platelets might be more likely to adhere and to cohere with each other, eventually leading to thrombus formation distal to the carotid web.

A limitation of our study is the small number of evaluated patients. This is partly due to the low prevalence of carotid webs. However, we also excluded three patients for CFD analysis due to poor 3D segmentation caused by insufficient imaging quality of the CTA scan. Thereby, statistical power of our analysis is limited and results must be interpreted with care. Secondly, due to the retrospective study design only data from CTA scans was available which resulted in missing patient-specific boundary conditions. For this reason, in- and outlet properties were estimated and generalized for all our patients [22]. None of our patients had an significant (>50%) stenosis in both carotid arteries, suggesting that the assumed flow ratio between ICA/CCA and ECA/CCA would be more reliable compared to estimations based on Murray's law [31]. Further studies on flow patterns of carotid webs, could overcome this problem by measuring blood flow with phase contrast magnetic resonance imaging (PC-MRI) scans [32]. In addition, patient specific waveform can be determined instead of generic wave forms as in the current study. Furthermore, turbulence models were not considered in our study despite the presence of a stenosis caused by the carotid web. However, previous research has shown that flow instabilities might occur under these conditions, but turbulence is not expected to occur [33].

Recent studies showed that carotid webs might be associated with acute ischemic stroke in younger patients without cardiovascular risk factors [34-36]. The results of the simulated flow patterns in the current study might be helpful in defining a therapeutic strategy for evaluation. Despite the use of antithrombotic agents, patients with a carotid web have a high risk of recurrent stroke [2, 3]. However, thrombus formation in carotid web might be comparable to thrombus formation in atrial appendage which is currently treated with oral anticoagulants [37]. Other potential treatment strategies of carotid webs are endovascular treatment (e.g. carotid angioplasty or stenting) or carotid endarterectomy [1, 38, 39].

Conclusions

In conclusion, carotid webs are associated with considerable recirculation zones and regional increased WSS. These findings suggest that a carotid web might stimulate thrombus formation which increases the risk of acute ischemic stroke.

REFERENCES

1. Choi PM, Singh D, Trivedi A, Qazi E, George D, Wong J, et al. Carotid webs and recurrent ischemic strokes in the era of ct angiography. *AJNR Am J Neuroradiol*. 2015;36:2134-2139
2. Joux J, Chausson N, Jeannin S, Saint-Vil M, Mejdoubi M, Hennequin JL, et al. Carotid-bulb atypical fibromuscular dysplasia in young afro-caribbean patients with stroke. *Stroke*. 2014;45:3711-3713
3. Haussen DC, Grossberg JA, Bouslama M, Pradilla G, Belagaje S, Bianchi N, et al. Carotid web (intimal fibromuscular dysplasia) has high stroke recurrence risk and is amenable to stenting. *Stroke*. 2017;48:3134-3137
4. Malek AM, Alper SL, Izumo S. Hemodynamic shear stress and its role in atherosclerosis. *JAMA*. 1999;282:2035-2042
5. Sui B, Gao P, Lin Y, Gao B, Liu L, An J. Blood flow pattern and wall shear stress in the internal carotid arteries of healthy subjects. *Acta Radiol*. 2008;49:806-814
6. Perktold K, Resch M, Florian H. Pulsatile non-newtonian flow characteristics in a three-dimensional human carotid bifurcation model. *J Biomech Eng*. 1991;113:464-475
7. Kamenskiy AV, Dzenis YA, Mactaggart JN, Desyatova AS, Pipinos, II. In vivo three-dimensional blood velocity profile shapes in the human common, internal, and external carotid arteries. *J Vasc Surg*. 2011;54:1011-1020
8. Cebral JR, Yim PJ, Lohner R, Soto O, Choyke PL. Blood flow modeling in carotid arteries with computational fluid dynamics and mr imaging. *Acad Radiol*. 2002;9:1286-1299
9. Lee SE, Lee SW, Fischer PF, Bassiouny HS, Loth F. Direct numerical simulation of transitional flow in a stenosed carotid bifurcation. *J Biomech*. 2008;41:2551-2561
10. Stroud JS, Berger SA, Saloner D. Numerical analysis of flow through a severely stenotic carotid artery bifurcation. *J Biomech Eng*. 2002;124:9-20
11. Steinman DA, Thomas JB, Ladak HM, Milner JS, Rutt BK, Spence JD. Reconstruction of carotid bifurcation hemodynamics and wall thickness using computational fluid dynamics and mri. *Magn Reson Med*. 2002;47:149-159
12. Marshall I, Zhao S, Papathanasopoulou P, Hoskins P, Xu Y. Mri and cfd studies of pulsatile flow in healthy and stenosed carotid bifurcation models. *J Biomech*. 2004;37:679-687
13. Lancellotti RM, Vergara C, Valdettaro L, Bose S, Quarteroni A. Large eddy simulations for blood dynamics in realistic stenotic carotids. *Int J Numer Method Biomed Eng*. 2017;33
14. Carallo C, Lucca LF, Ciamei M, Tucci S, de Franceschi MS. Wall shear stress is lower in the carotid artery responsible for a unilateral ischemic stroke. *Atherosclerosis*. 2006;185:108-113
15. Peiffer V, Sherwin SJ, Weinberg PD. Computation in the rabbit aorta of a new metric - the transverse wall shear stress - to quantify the multidirectional character of disturbed blood flow. *J Biomech*. 2013;46:2651-2658
16. Mohamied Y, Sherwin SJ, Weinberg PD. Understanding the fluid mechanics behind transverse wall shear stress. *J Biomech*. 2017;50:102-109
17. He X, Ku DN. Pulsatile flow in the human left coronary artery bifurcation: Average conditions. *J Biomech Eng*. 1996;118:74-82
18. Cheng C, Tempel D, van Haperen R, van der Baan A, Grosveld F, Daemen MJ, et al. Atherosclerotic lesion size and vulnerability are determined by patterns of fluid shear stress. *Circulation*. 2006;113:2744-2753
19. Berkhemer OA, Fransen PS, Beumer D, van den Berg LA, Lingsma HF, Yoo AJ, et al. A randomized trial of intraarterial treatment for acute ischemic stroke. *N Engl J Med*. 2015;372:11-20
20. Horos Project. Dicom image viewing and measuring. *Horos*.http://www.horosproject.org/

21. Cheng C, Helderman F, Tempel D, Segers D, Hierck B, Poelmann R, et al. Large variations in absolute wall shear stress levels within one species and between species. *Atherosclerosis*. 2007;195:225-235
22. Groen HC, Simons L, van den Bouwhuijsen QJ, Bosboom EM, Gijsen FJ, van der Giessen AG, et al. Mri-based quantification of outflow boundary conditions for computational fluid dynamics of stenosed human carotid arteries. *J Biomech*. 2010;43:2332-2338
23. Seo T, Schachter LG, Barakat AI. Computational study of fluid mechanical disturbance induced by endovascular stents. *Ann Biomed Eng*. 2005;33:444-456
24. Lee SW, Antiga L, Spence JD, Steinman DA. Geometry of the carotid bifurcation predicts its exposure to disturbed flow. *Stroke*. 2008;39:2341-2347
25. Schrauwen JT, Karanasos A, van Ditzhuijzen NS, Aben JP, van der Steen AF, Wentzel JJ, et al. Influence of the accuracy of angiography-based reconstructions on velocity and wall shear stress computations in coronary bifurcations: A phantom study. *PLoS One*. 2015;10:e0145114
26. Schoephoerster RT, Oynes F, Nunez G, Kapadvanjwala M, Dewanjee MK. Effects of local geometry and fluid dynamics on regional platelet deposition on artificial surfaces. *Arterioscler Thromb*. 1993;13:1806-1813
27. Slager CJ, Wentzel JJ, Gijsen FJ, Thury A, van der Wal AC, Schaar JA, et al. The role of shear stress in the destabilization of vulnerable plaques and related therapeutic implications. *Nat Clin Pract Cardiovasc Med*. 2005;2:456-464
28. Botnar R, Rappitsch G, Scheidegger MB, Liepsch D, Perktold K, Boesiger P. Hemodynamics in the carotid artery bifurcation: A comparison between numerical simulations and in vitro mri measurements. *J Biomech*. 2000;33:137-144
29. Chatzizisis YS, Coskun AU, Jonas M, Edelman ER, Feldman CL, Stone PH. Role of endothelial shear stress in the natural history of coronary atherosclerosis and vascular remodeling: Molecular, cellular, and vascular behavior. *J Am Coll Cardiol*. 2007;49:2379-2393
30. Zhang Q, Gao B, Gu K, Chang Y, Xu J. The study on hemodynamic effect of varied support models of bjut-ii vad on coronary artery: A primary cfd study. *ASAIO J*. 2014;60:643-651
31. Sherman TF. On connecting large vessels to small. The meaning of murray's law. *J Gen Physiol*. 1981;78:431-453
32. von Schulthess GK, Higgins CB. Blood flow imaging with mr: Spin-phase phenomena. *Radiology*. 1985;157:687-695
33. Gijsen FJ, Palmen DE, van der Beek MH, van de Vosse FN, van Dongen ME, Janssen JD. Analysis of the axial flow field in stenosed carotid artery bifurcation models--lda experiments. *J Biomech*. 1996;29:1483-1489
34. Pereira BJA, Batista UC, Tosello RT, Stroher IN, Baeta AM, Piske RL. Web vessels: Literature review and neurointerventional management. *World Neurosurg*. 2018;110:e907-e916
35. Compagne KCJ, van Es A, Berkhemer OA, Borst J, Roos Y, van Oostenbrugge RJ, et al. Prevalence of carotid web in patients with acute intracranial stroke due to intracranial large vessel occlusion. *Radiology*. 2018;286:1000-1007
36. Coutinho JM, Derkatch S, Potvin AR, Tomlinson G, Casaubon LK, Silver FL, et al. Carotid artery web and ischemic stroke: A case-control study. *Neurology*. 2017;88:65-69
37. Kirchhof P, Benussi S, Kotecha D, Ahlsson A, Atar D, Casadei B, et al. 2016 esc guidelines for the management of atrial fibrillation developed in collaboration with eacts. *Rev Esp Cardiol (Engl Ed)*. 2017;70:50

38. Elmokadem AH, Ansari SA, Sangha R, Prabhakaran S, Shaibani A, Hurley MC. Neurointerventional management of carotid webs associated with recurrent and acute cerebral ischemic syndromes. *Interv Neuroradiol*. 2016;22:432-437
39. Brinjikji W, Agid R, Pereira VM. Carotid stenting for treatment of symptomatic carotid webs: A single-center case series. *Interv Neurol*. 2018;7:233-240

Suppl. Table 1. Results of the CFD simulation of carotid bifurcations

	Recirculation zone										*At level of the carotid bulbus*		
Case	Area *(mm^2)*		Length *(mm)*		Mean TAWSS *(Pa)*		Maximum transWSS *(Pa)*		Maximum OSI		Stenosis on CTA % *(ECST)*		Maximum TAWSS *(Pa)*
	web	control	web	control	web	control	web	control	web	control	web	control	web
1	63.61	58.95	8.6	2.1	0.17	0.15	0.13	0.10	0.41	0.18	27	0	0.37
2	60.33	36.46	5.6	1.4	0.30	0.26	0.33	0.30	0.35	0.38	23	0	0.54
3	46.48	36.94	2.3	1.4	0.77	0.28	0.58	0.21	0.36	0.17	45	11	1.29
4	50.60	16.51	2.0	1.1	0.24	0.27	0.25	0.05	0.37	0.23	26	0	0.34
5	224.04	94.71	17.7	2.3	0.15	0.28	0.18	0.16	0.48	0.33	49	28	0.58
6	99.38	48.60	8.3	2.1	0.34	0.22	0.20	0.23	0.43	0.40	26	0	0.61
7	87.18	31.30	6.9	1.8	0.23	0.28	0.26	0.21	0.48	0.31	30	7	0.61
8	100.63	50.34	8.7	1.8	0.27	0.14	0.22	0.10	0.39	0.19	27	4	0.51
9	30.92	43.01	5.9	1.8	0.59	0.33	0.31	0.26	0.27	0.30	37	23	0.88

Hemodynamic characteristics of all individual subjects based on computational fluid dynamics (CFD) simulation and CT angiography. All patients had a carotid web in the carotid bifurcation at the symptomatic side of acute ischemic stroke except case 9.

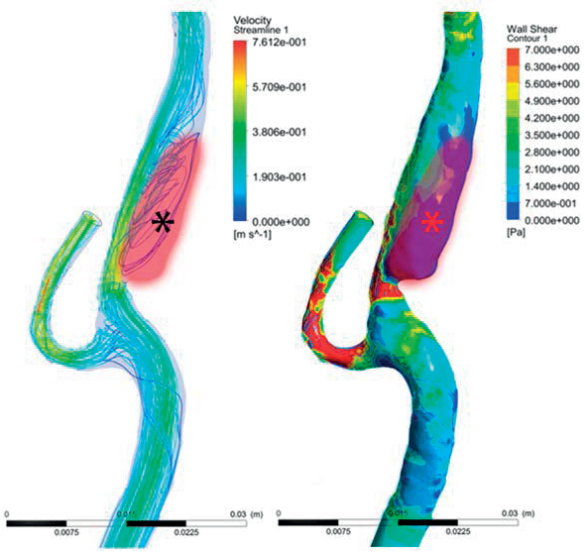

Suppl. Figure 1. Marked locations where TAWSS and OSI were assessed.

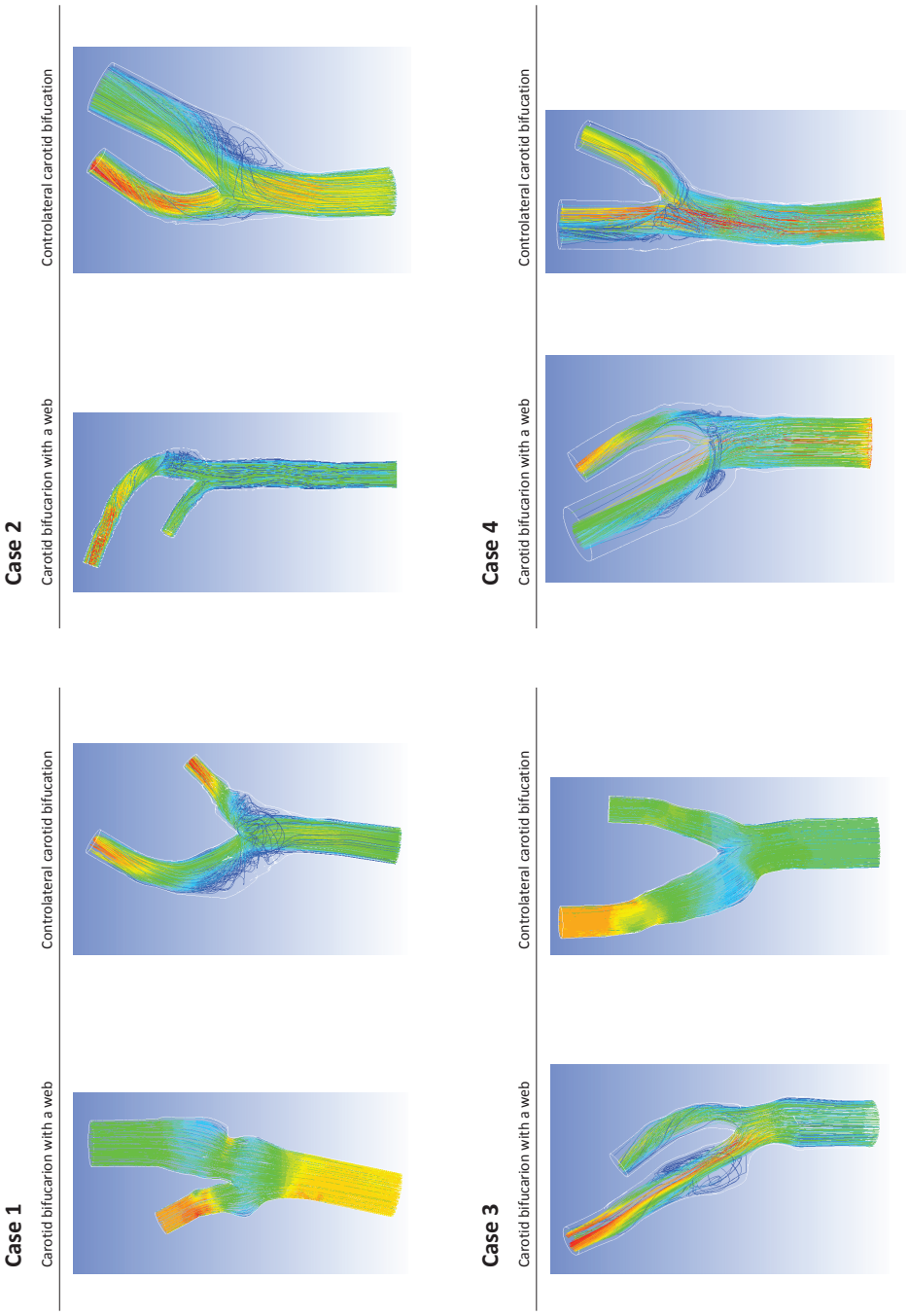

Suppl. Figure 2.

Case 5

Carotid bifucarion with a web

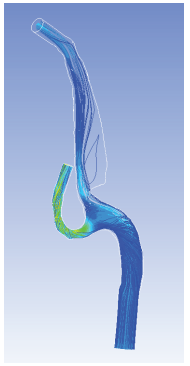

Controlateral carotid bifucation

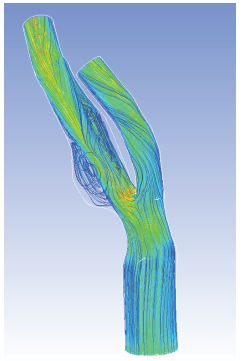

Case 6

Carotid bifucarion with a web

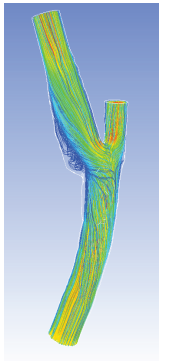

Controlateral carotid bifucation

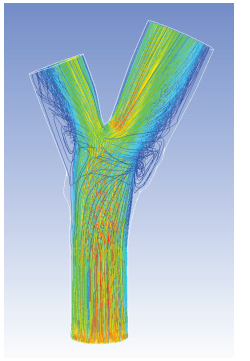

Case 7

Carotid bifucarion with a web

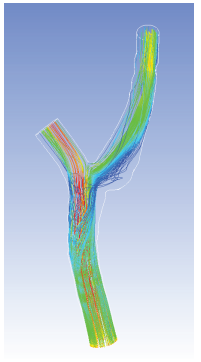

Controlateral carotid bifucation

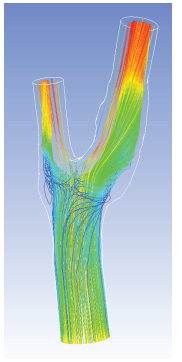

Case 8

Carotid bifucarion with a web

Controlateral carotid bifucation

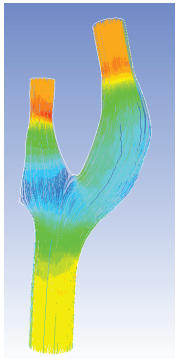

Case 9

Carotid bifucarion with a web

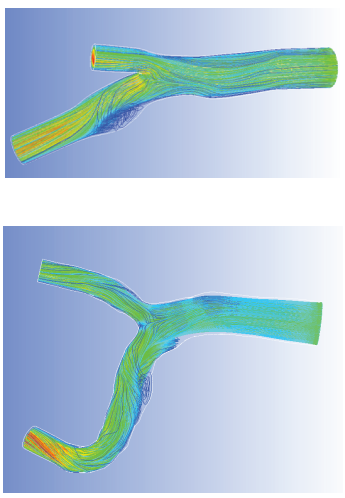

Controlateral carotid bifucation